

DMAligner: Enhancing Image Alignment via Diffusion Model Based View Synthesis

Xinglong Luo^{1,2}, Ao Luo³, Zhengning Wang^{1†},
Yueqi Yang⁴, Chaoyu Feng⁴, Lei Lei⁴, Bing Zeng¹, and Shuaicheng Liu^{1†}

¹University of Electronic Science and Technology of China

²Qianyuan Laboratory, Hangzhou, China ³Southwest Jiaotong University ⁴Independent Researcher
{xinglong.luo@std., zhengning.wang@, eezeng@, liushuaicheng@}uestc.edu.cn aoluo@swjtu.edu.cn

Abstract

Image alignment is a fundamental task in computer vision with broad applications. Existing methods predominantly employ optical flow-based image warping. However, this technique is susceptible to common challenges such as occlusions and illumination variations, leading to degraded alignment visual quality and compromised accuracy in downstream tasks. In this paper, we present DMAligner, a diffusion-based framework for image alignment through alignment-oriented view synthesis. DMAligner is crafted to tackle the challenges in image alignment from a new perspective, employing a generation-based solution that showcases strong capabilities and avoids the problems associated with flow-based image warping. Specifically, we propose a Dynamics-aware Diffusion Training approach for learning conditional image generation, synthesizing a novel view for image alignment. This incorporates a Dynamics-aware Mask Producing (DMP) module to adaptively distinguish dynamic foreground regions from static backgrounds, enabling the diffusion model to more effectively handle challenges that classical methods struggle to solve. Furthermore, we develop the Dynamic Scene Image Alignment (DSIA) dataset using Blender, which includes 1,033 indoor and outdoor scenes with over 30K image pairs tailored for image alignment. Extensive experimental results demonstrate the superiority of the proposed approach on DSIA benchmarks, as well as on a series of widely-used video datasets for qualitative comparisons. Our code is available at <https://github.com/boomluo02/DMAligner>.

1. Introduction

The alignment of consecutive frames is a critical task in computer vision, supporting a wide range of applications

[†] Corresponding Author.

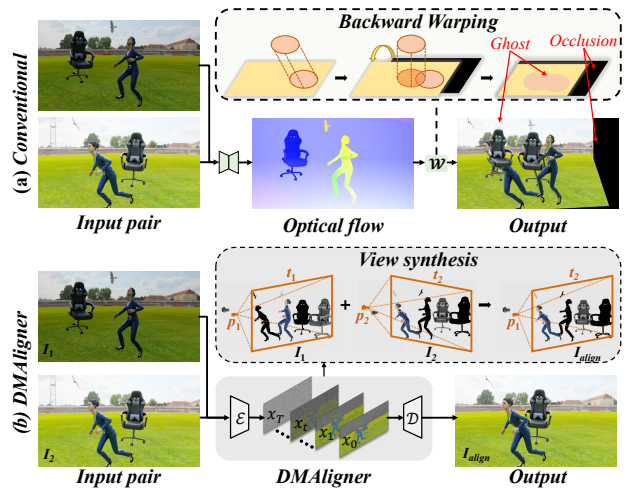


Figure 1. (a) Conventional image alignment based on optical flow and image warping, resulting in ghosting artifacts and occlusion. (b) Our DMAligner directly generates the complete alignment image via diffusion-based view synthesis.

such as High-Dynamic-Range (HDR) imaging [49], image deblurring [52], burst image restoration [8], under-display camera imaging [7], video super-resolution [3], video denoising [55] and video stabilization [22]. Precise alignment ensures the accurate merging of information from consecutive frames, leading to enhanced image quality and better performance in subsequent tasks [35, 46]. Despite its significance, the task of image alignment remains challenging due to various factors, including scene dynamics, large camera motion, and varying lighting conditions.

Recent advancements in deep learning have led to substantial progress in neural network-based alignment methods. Generally, image alignment can be divided into three levels: global-level, mid-level, and pixel-level alignment. Global-level alignment typically involves estimating a homography matrix, which can be accomplished using unsu-

pervised deep learning frameworks [21]. This technique effectively aligns images under conditions of planar scenes or when the camera undergoes basic rotational or translational motion. Moreover, through global-to-local homography flow refinement, it can be naturally extended to local mesh-grid homography estimation [20], allowing it to overcome the limitations of a single homography [21]. However, global- and mid-level methods are restricted in their ability to address more complex scenarios, like parallax, non-rigid deformations, or significant foreground motion, since they assume single or multiple global transformations across the entire image.

Another prominent technique involves the pixel-level approaches with optical flow and image warping [1]. Despite progress in image alignment, current optical flow-based methods face challenges that limit their effectiveness in practical applications. A major issue is the sensitivity of optical flow methods to brightness changes. Variations in lighting conditions, such as shadows, reflections, or changes in ambient light, can significantly distort the brightness constancy assumption, leading to incorrect motion estimation. Besides, the warping process inherent in optical flow-based alignment can introduce various artifacts. Inaccuracies in the motion field can lead to distortions such as stretching, compressing, or tearing of image regions. Additionally, the many-to-one mapping inherent in image warping on occlusion regions inevitably results in ghosting artifacts, as depicted in Fig. 1 (a), even with precise optical flow estimation. Such artifacts not only degrade the visual quality of the aligned frames but also affect the accuracy of subsequent processing tasks.

In this paper, we introduce DMAligner, a diffusion-based framework for image alignment through alignment-oriented view synthesis. As depicted in Fig. 2, the desired image alignment result represents a scenario where the camera pose stays fixed at P_1 while time advances from t_1 to t_2 . DMAligner is designed to handle the challenges in image alignment from a new perspective with a generation-based solution (see Fig. 1 (b)), exhibiting strong capabilities and avoiding issues associated with homography and flow-based image warping. Specifically, we first create Dynamic Scene Image Alignment (DSIA) dataset, designed to simulate typical image alignment challenges including camera shifts, moving objects, and fluctuating illumination. Moreover, we propose the Dynamics-aware Diffusion Training approach on the Latent Diffusion Model (LDM) [40] for learning conditional image generation. The key idea is to enhance the network’s capacity to recognize dynamic information during diffusion model training. This is realized through the Dynamics-aware Mask Producing (DMP) module, which effectively discriminates dynamic foreground regions from static backgrounds within the hidden features across frames. Additionally, we validate the effectiveness of

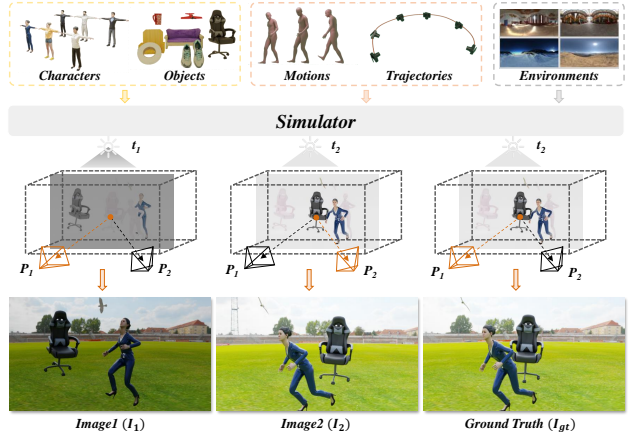


Figure 2. Overview of DSIA dataset generation. The ground truth image is rendered by setting the time to t_2 and the camera pose to P_1 , where the background statics mirror those in I_1 , and the dynamics are akin to I_2 , with slight visualization variances caused by pose changes. As a result, I_{gt} can be regarded as the *alignment-oriented view synthesis* with reference from I_2 to I_1 (i.e., I_2' for I_2 to I_1 alignment).

DMAligner through extensive testing on synthetic datasets, including the proposed DSIA and Sintel [2], as well as on the widely-used real-world dataset DAVIS [36]. Both the quantitative and qualitative results demonstrate significant enhancements over contemporary methods. The contributions are summarized as follows:

- We develop **DSIA** dataset, the first large-scale dataset specific for image alignment, which simulates the typical challenges including camera motion, moving objects, and changes in illumination.
- We present **DMAligner**, a novel diffusion-based framework for image alignment via alignment-oriented view synthesis. The central idea is to enhance the network’s capability to capture dynamic information during diffusion model training, with the assistance of our **DMP** module.
- The proposed method achieves **state-of-the-art performance** on DSIA benchmarks and also demonstrates the **superior generalization capability** on both synthetic and real-world datasets.

2. Related Work

Image Alignment. Traditional approaches primarily rely on feature-based methods, where keypoints are detected and matched across images, followed by geometric transformation estimation to align the images [18]. In the deep learning era, deep convolutional neural networks (DCNNs) have revolutionized image alignment in feature space [23]. Furthermore, the Transformer has also been utilized for feature-domain alignment, extending their application beyond standard RGB images [4] to directly process RAW

image data [37, 39]. In image space, Global- and middle-level alignments typically involve estimating a homography matrix [21] and local mesh-grid homography [20], respectively. But they cannot handle complex scenarios, involving parallax, non-rigid deformations, or significant foreground motion. A notable advancement in image alignment is the adoption of optical flow-based image warping techniques. Optical flow calculates pixel-wise motion between consecutive images, enabling the warping of one image to align with another. With the advances of recent optical flow approaches [6, 27, 30], this method has found widespread use across a variety of video-based applications [24, 56]. Despite their success, warping in occlusion regions inevitably leads to ghosting artifacts, even with accurate flow, as shown in Fig. 1. In contrast, our DMAligner addresses the challenges in image alignment from a new perspective, performing *alignment-oriented view synthesis* using a diffusion-based framework.

Diffusion Model. Diffusion models [11, 40, 43] own prominent generative performance for synthesis, and various approaches have been developed to improve the performance or efficiency. Different applications have shown good performances when empowered with diffusion models, including but not limited to, optical flow estimation [28], homography estimation [16], shadow removal [29], image rectangling [60], rolling shutter removal [51], HDR image reconstruction [25], low-light image enhancement [12, 13], raw image processing [26, 38], camouflaged object detection [58] and robot manipulation [5, 47, 48, 57]. In this work, we propose an end-to-end diffusion-based framework that *specifically handles cross-frame dynamic information* for image alignment.

3. Method

3.1. DSIA Dataset Generation

To the best of our knowledge, *there is no large-scale dataset that addresses the specific challenges of image alignment, such as camera motion, moving objects, and varying illumination, while also providing corresponding ground truth images.* To fill this gap, we create the Dynamic Scene Image Alignment (DSIA) dataset, which simulates these challenges and includes 1,033 indoor and outdoor scenes with over 30K image pairs at a resolution of 960×540 . The main idea is to *simulate the burst image capturing processes with the moving camera across a variety of dynamic scenes.* Fig. 2 illustrates the overview of DSIA dataset generation.

Specifically, inspired by PointOdyssey [59] and Kubric [10], we assemble 25 characters and 100 objects with diverse shapes and materials from several open-source sources, including BlenderKit, Mixamo, GSO, and PartNet. These characters are animated using real-world motion

capture data, while the locations and rotations of object poses are randomly adjusted to simulate real-world motion. Camera motion is controlled along predefined trajectories extracted from [17]. By collecting and animating these assets (characters, objects, and cameras), we generate 3D virtual scenes that closely mimic real-world dynamics. These scenes are then rendered with the Blender engine, producing image sequences $\{I_1, I_2, \dots, I_N\}$, in which characters, objects, and the camera all move simultaneously. To maximize the diversity of the generated images, we randomly introduce HDR environments with various materials, textures, and lighting conditions.

We systematically rearrange the sequencing of the camera trajectories relative to character and object motions, capturing dynamic scenes from various positions along the trajectories, and rendering to generate virtual viewpoint images tailored for image alignment. Considering two consecutive images, I_1 and I_2 involve both global camera motion \mathcal{H} and local foreground movement \mathcal{F} . Their transformations can be described using the traditional warp operation \mathcal{W} :

$$I_1 = \mathcal{W}(I_2) + \mathcal{T} = \mathcal{H}(\mathcal{F}(I_2)) + \mathcal{T}, \quad (1)$$

where \mathcal{T} represents the changes in image texture. In our approach, we capture the dynamic scene at the time of I_2 from the camera viewpoint of I_1 , generating the aligned image I_{gt} as Ground Truth. Compared to I_1 , I_{gt} involves local foreground movement \mathcal{F} , while compared to I_2 , I_{gt} involves global camera motion \mathcal{H} :

$$I_{gt} = \mathcal{H}(I_2) = \mathcal{F}(I_1) + \mathcal{T}. \quad (2)$$

The dataset is divided into four subsets based on varying camera and foreground movements.

3.2. Diffusion Model for Image Alignment

3.2.1. Overview.

The training and inference pipelines of our DMAligner are depicted in Fig. 3. The entire process is formulated in the latent space using LDM [40]. The core insight is to equip the network with the ability to capture dynamic information during diffusion model training. This is accomplished by the Dynamics-aware Mask Producing (DMP) module, which effectively differentiates dynamic foreground regions from static backgrounds within the cross-frame hidden features. We elaborate on the model training and inference details in the following subsections.

3.2.2. Dynamics-aware Diffusion Training.

Given a set of image data I_1 , I_2 , and I_{gt} , we follow LDM [40] to transform these high-resolution images into the latent representational space using a perceptual compression model based on the encoder-decoder architecture,

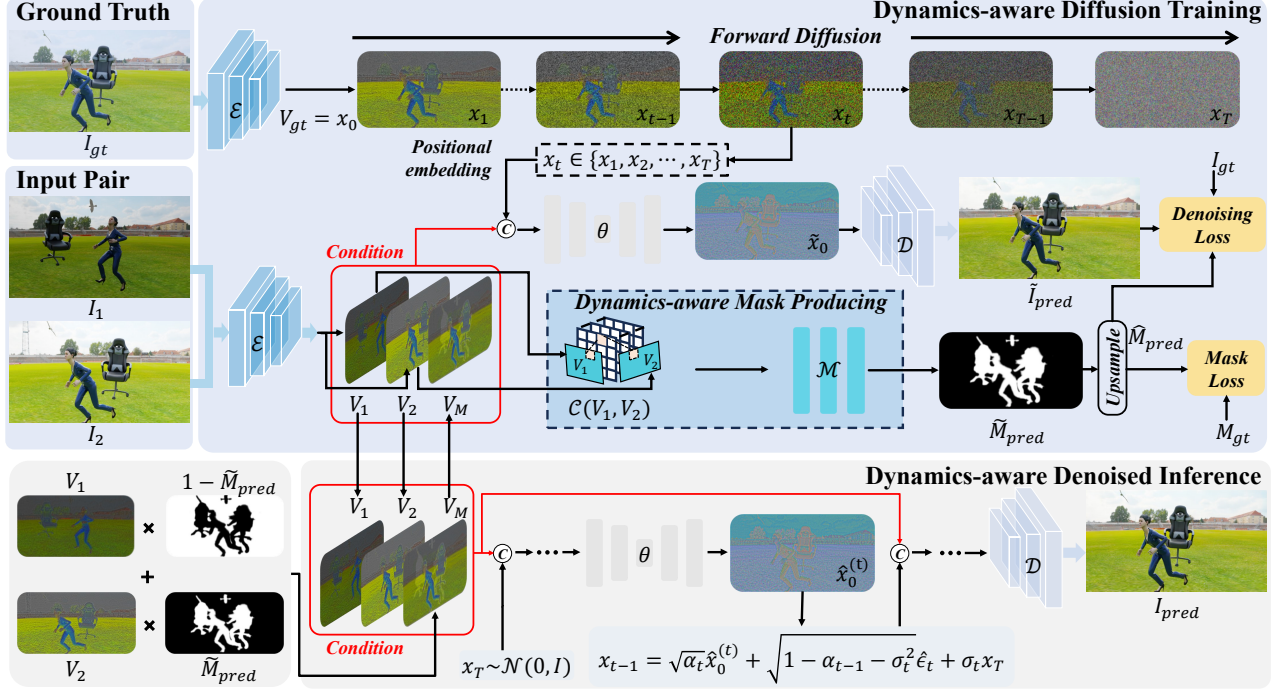


Figure 3. Overview of our DMAligner. Instead of using the discriminative learning paradigm for optical flow estimation and image warping, our framework employs a generative approach to achieve image alignment with a diffusion model. Dynamics-aware Mask Producing (DMP) module is crucial for providing dynamic information, essential for performing the Dynamics-aware Diffusion Training process in this task.

and then reconstruct them back into RGB images. Specifically, for I_{gt} , the encoder \mathcal{E} encodes it into the latent representation V_{gt} , and the decoder \mathcal{D} reconstructs it into the RGB image:

$$\tilde{I}_{gt} = \mathcal{D}(V_{gt}) = \mathcal{D}(\mathcal{E}(I_{gt})). \quad (3)$$

The same process is applied to I_1 and I_2 , resulting in latent representations V_1 and V_2 . We use V_1 and V_2 as the condition in the latent representational space and train the diffusion model θ to learn sampling from standard Gaussian noise, generating the latent that matches the distribution of V_{gt} . Our training scheme consists of four components: Forward Diffusion, Conditional Learning, Dynamics-aware Mask Producing, and Loss Function.

Forward Diffusion: As illustrated in Fig. 3, we apply different timesteps t to add varying levels of noise to V_{gt} (denoted as x_0), generating a series of noise representations $x_t \in \{x_1, x_2, \dots, x_T\}$. x_t indicates any noise representation at a specific timestep t , and as t increases, the level of added noise grows, leading to an increase in the entropy of the distribution of x_t . Ultimately, the distribution becomes standard Gaussian noise, $x_T \sim \mathcal{N}(0, 1)$, defined as:

$$x_t \in \{x_1, x_2, \dots, x_T\}, x_T \sim \mathcal{N}(0, 1), x_0 = V_{gt}. \quad (4)$$

The forward diffusion process typically follows the approach of [11], where Gaussian noise is incrementally

added to the data sample based on a Markov chain. This allows for the diffusion from x_0 to any timestep x_t in one step using the following equation:

$$q(x_t | x_0) = \mathcal{N}(x_t | \sqrt{\bar{\alpha}_t}x_0, (1 - \bar{\alpha}_t)I), \quad (5)$$

where $\bar{\alpha}_t$ represents the cumulative product of a set of predefined noise variance schedules $\{\beta_1, \beta_2, \dots, \beta_t\}$, which ensures that the noise incrementally increases with t , defined as $\bar{\alpha}_t := \prod_{i=1}^t \alpha_i = \prod_{i=1}^t (1 - \beta_i)$.

Dynamics-aware Mask Producing: To explicitly guide the denoising network to focus on moving foreground objects and enhance local detail reconstruction, we utilize a motion mask. First, we extract motion information by computing a normalized dot-product cost volume \mathcal{C} between latents V_1 and V_2 . For a spatial coordinate \mathbf{u} and a displacement \mathbf{d} , the correlation is defined as:

$$\mathcal{C}\{\mathbf{u}, \mathbf{d}\} = \frac{1}{N} \sum_{k=1}^N V_1^{(k)}(\mathbf{u}) \cdot V_2^{(k)}(\mathbf{u} + \mathbf{d}), \quad (6)$$

where N is the channel dimension. Assuming the input images I_1 and I_2 have a spatial resolution of $\mathbb{R}^{3 \times H \times W}$ and the encoder \mathcal{E} has a downsampling factor of s , the resulting latents V_1 and V_2 both belong to $\mathbb{R}^{N \times \frac{H}{s} \times \frac{W}{s}}$. Consequently, the correlation volume $\mathcal{C} \in \mathbb{R}^{D^2 \times \frac{H}{s} \times \frac{W}{s}}$ (where D represents the maximum displacement) is fed into a mask

Table 1. Comparison of network inputs among DPFlow [34], COGS [14], AccidentalGS [33], GenWarp [41] and our DMA-aligner. Other optical flow networks (PWCNet [44], RAFT [45], FlowFormer++ [42], FlowDiffuser [28]) have the same input structure as DPFlow.

Method	Input Structure
DPFlow [34]	2 images (I_1, I_2)
COGS [14]	2 images (I_1, I_2) + Depth (D_1, D_2) + Mask (M_1, M_2)
AccidentalGS [33]	2 images (I_1, I_2) + Depth (D_1, D_2) + Camera Intrinsic (K)
GenWarp [41]	Single image (I_2) + Camera Intrinsic (K) + Depth (D_2) + Camera Motion ($P_{I_2 \rightarrow I_1}$)
DMA-aligner	2 images (I_1, I_2)

predictor \mathcal{M} to generate the motion mask $\tilde{M}_{pred} = \mathcal{M}(C)$. To ensure smooth visual transitions at object boundaries, we expand this mask using a dilation operation d_r (which is fully differentiable and implemented via the PyTorch “torch.nn.functional.max_pool2d” operation with a stride of 1). The dilated mask is subsequently used to fuse the background of V_1 with the foreground of V_2 :

$$V_M = V_2 \odot d_r(\tilde{M}_{pred}) + V_1 \odot \{1 - d_r(\tilde{M}_{pred})\}. \quad (7)$$

This mixed latent V_M serves as a critical conditioning signal to guide the diffusion network in generating the final aligned output.

Conditional Learning: As shown in Fig. 3, we concatenate V_1 , V_2 and V_M along the channel dimension to form the condition x_{cond} , then randomly select x_t from the noise representations $\{x_1, x_2, \dots, x_T\}$, allowing the diffusion model θ to learn the denoising process. This enables θ to handle any x_t at an arbitrary timestep t , producing a denoised output \hat{x}_0 . Similar to approaches in [28], we use the “predict x_0 ” denoising setting in our model. The condition x_{cond} is concatenated with x_t and the encoded timestep t through positional embedding (PE), and the resulting tensor is sent to the diffusion model to obtain the denoised result \tilde{x}_0 :

$$\tilde{x}_0 = \theta([x_t, x_{cond}, PE(t)]), \quad (8)$$

then \tilde{x}_0 is reconstructed to become \tilde{I}_{pred} by decoder \mathcal{D} , which can be expressed as $\tilde{I}_{pred} = \mathcal{D}(\tilde{x}_0)$. Experiments demonstrate that “predict x_0 ” is more effective for image alignment compared to others.

Loss Function: Our model directly learns to denoise and reconstruct a latent representation \tilde{x}_0 from x_t that matches the distribution of V_{gt} . Then, it is decoded by \mathcal{D} into the RGB image \tilde{I}_{pred} , supervised by I_{gt} in the image domain to ensure reliable and accurate output. Additionally, the trainer learns the motion foreground mask \tilde{M}_{pred} , which is then upsampled to obtain \hat{M}_{pred} , helping the model to focus on regions with significant variance. The denoising loss

function, namely Denoising Loss, is defined as follows:

$$\hat{M}_{pred} = Upsample\{d_r(\tilde{M}_{pred})\}, \quad (9)$$

$$L_{Denoising} = (1 - \gamma) \left\| (1 - \hat{M}_{pred})(I_{gt} - I_{pred}) \right\|_2 + \gamma \left\| (\hat{M}_{pred})(I_{gt} - I_{pred}) \right\|_2, \quad (10)$$

where γ is a variable weighting coefficient, and d_r represents the dilation operation applied to the mask r times. We also supervise the mask \tilde{M}_{pred} using the cross-entropy loss, referred to as the Mask Loss:

$$L_{Mask} = -M_{gt} \log(\hat{M}_{pred}) - (1 - M_{gt}) \log(1 - \hat{M}_{pred}). \quad (11)$$

The total loss is:

$$L_{Total} = \lambda_1 L_{Denoising} + \lambda_2 L_{Mask}. \quad (12)$$

In our experiments, the downsampling factor of s , the parameters r (in d_r), λ_1 , and λ_2 are set to 4, 2, 2, and 0.1, respectively.

3.2.3. Dynamics-aware Denoised Inference.

After training, the diffusion model θ performs inference by denoising a standard Gaussian noise $x_T \in \mathcal{N}(0, 1)$, conditioned on V_1 , V_2 and V_M . This process reconstructs a reliable and accurate alignment result through recurrent denoising. Specifically, the model θ takes x_T , the condition, and the timestep T as inputs according to Eq. (8), producing an initial coarse denoised output $\hat{x}_0^{(T)}$. Then, following the non-Markovian forward process [43] parametrized by σ as shown in Eq. (13), it generates x_{T-1} at timestep $T - 1$. This process is repeated recurrently, producing a sequence of progressively refined denoised results $\hat{x}_0^{(T)}, \hat{x}_0^{(T-1)}, \dots, \hat{x}_0^{(1)}$. Finally, $\hat{x}_0^{(1)}$ is passed through the decoder \mathcal{D} to output the aligned image I_{pred} . The non-Markovian forward process is defined as:

$$x_{t-1} = \sqrt{\alpha_{t-1}} \hat{x}_0^{(t)} + \sqrt{1 - \alpha_{t-1} - \sigma_t^2} \hat{\epsilon}_t + \sigma_t x_T, \quad (13)$$

where $\hat{x}_0^{(t)}$ is the prediction of x_0 from x_t using the diffusion model θ , and $\hat{\epsilon}_t$ is the approximate noise calculated by

$$\hat{\epsilon}_t = \frac{x_t - \sqrt{\alpha_t} \hat{x}_0^{(t)}}{\sqrt{1 - \alpha_t}}. \quad (14)$$

In the recurrent update process described above, the step size Δ is not fixed and can be adjusted to other values. By setting an appropriate step size Δ , inference can be accelerated while still allowing incremental refinement of the results. The iterative update process can be expressed as: $\{x_T \rightarrow \hat{x}_0^{(T)}\} \rightarrow \{x_{T-\Delta} \rightarrow \hat{x}_0^{(T-\Delta)}\} \rightarrow \dots \rightarrow \{x_1 \rightarrow \hat{x}_0^{(1)}\}$. In our empirical analysis, we set $T = 1000$ and $\Delta = 20$.



Figure 4. Qualitative comparisons between DPFlow [34], COGS [14], GenWarp [41] and our DMAligner on our DSIA dataset.

Table 2. Quantitative comparison on our DSIA dataset across four subsets (LcLf, LcSf, ScLf, and ScSf) using PSNR and SSIM metrics, *higher scores indicate better performance*. The average (“Avg”) across all subsets summarizes overall results. † indicates that occlusion and ghost regions are excluded during metric computation, as determined by forward-backward consistency check [50].

Methods	LcLf		LcSf		ScLf		ScSf		Avg.	
	PSNR↑	SSIM↑								
<i>Methods based on Flow Warping</i>										
PWCNet [44]	16.53	0.74	16.40	0.73	20.53	0.74	21.01	0.76	18.62	0.74
RAFT [45]	18.22	0.74	18.34	0.74	22.46	0.77	22.95	0.76	20.49	0.75
FlowFormer++ [42]	21.02	0.75	20.97	0.76	22.84	0.77	23.94	0.79	22.19	0.77
FlowDiffuser [28]	20.18	0.75	20.33	0.75	23.39	0.78	23.91	0.79	21.95	0.77
DPFlow [34]	20.78	0.76	20.50	0.74	23.94	0.78	24.61	0.80	22.46	0.77
PWCNet† [44]	22.03	0.76	21.15	0.76	24.63	0.79	24.74	0.77	23.14	0.77
RAFT† [45]	22.99	0.78	23.15	0.77	25.07	0.80	25.09	0.79	24.08	0.78
FlowFormer++† [42]	24.19	0.79	24.24	0.78	25.61	0.81	25.74	0.81	24.95	0.80
FlowDiffuser† [28]	23.82	0.78	23.81	0.77	25.78	0.81	25.89	0.82	24.82	0.80
DPFlow† [34]	<u>24.30</u>	<u>0.79</u>	<u>24.84</u>	<u>0.79</u>	<u>25.99</u>	0.82	<u>26.04</u>	<u>0.82</u>	<u>25.29</u>	<u>0.81</u>
<i>Methods based on View Synthesis</i>										
COGS [14]	16.35	0.66	16.84	0.69	17.01	0.69	18.21	0.71	17.10	0.69
AccidentalGS [33]	17.47	0.68	19.12	0.70	20.38	0.71	21.33	0.74	19.58	0.71
SD-Inpaint [53]	22.14	0.75	22.92	0.76	25.42	0.79	25.77	0.81	24.06	0.78
GenWarp [41]	22.62	0.76	23.15	0.76	25.32	0.78	25.84	0.81	24.23	0.78
DMAligner (Ours)	24.91	0.80	26.90	0.81	27.25	<u>0.81</u>	27.64	0.83	26.67	0.81

4. Experiments

4.1. Input Structure

As detailed in Tab. 1, our DMAligner and DPFlow [34] are highly efficient, requiring only two consecutive frames (I_1, I_2) for alignment-oriented view synthesis and optical flow estimation, respectively. In contrast, 3DGS-based methods heavily depend on auxiliary priors for scene reconstruction. Beyond two input images (I_1 and I_2), COGS [14] requires depth maps (D_1, D_2) estimated by Marigold [15] and foreground masks (M_1, M_2) predicted by FC-CLIP [54]. AccidentalGS [33] similarly relies on two input images (I_1 and I_2), depth priors (D_1, D_2) and camera intrinsics (K). Furthermore, while GenWarp [41] claims single-image input (I_2), it implicitly requires both I_1 and I_2 to estimate relative camera motion $P_{I_2 \rightarrow I_1}$ via optical flow [19, 31, 32], alongside camera intrinsics (K) and depth (D_2) from Marigold [15]. Ultimately, unlike these geometry-dependent approaches, our DMAligner achieves

accurate alignment without requiring depth, masks, intrinsics, or pose transformations, offering a much simpler and more direct framework.

4.2. Implementation Details

Our DSIA dataset comprises 1,033 indoor and outdoor scenes with a resolution of 960×540 . The dataset is divided into a training set with over 30k samples and a test set with 2k samples. We partition the test set into four subsets based on the magnitude of camera and foreground motion: LcLf, LcSf, ScLf and ScSf (Lc: large camera motion, Lf: large foreground motion, Sc: small camera motion, Sf: small foreground motion). For the training phase, we initialize a VQ-VAE with pre-trained weights from LDM [40] and fine-tune it on our DSIA dataset. Subsequently, we freeze the VQ-VAE encoder and *train our custom denoising UNet from scratch* to address the alignment task. Training uses random 480×256 crops with flipping, while inference supports larger inputs on a single GPU.



Figure 5. Qualitative comparisons between DPFlow [34], GenWarp [41] and our DMAligner on Sintel dataset.



Figure 6. Qualitative comparisons between DPFlow [34], GenWarp [41] and our DMAligner on the real-world DAVIS dataset.

4.3. Comparison with Existing Methods

4.3.1. Results on DSIA.

Tab. 2 compares our DMAligner with some flow-warping methods and view-synthesis methods. In our DSIA dataset, all flow-warping methods are trained using rendered ground truth optical flow. We then align I_2 to I_{gt} using back warping and compute PSNR and SSIM between I_{pred} and I_{gt} . To address occlusion and ghosting artifacts from warping, these regions (determined by forward-backward consistency check [50]) are excluded from the metrics calculation, as marked by \dagger . Fig. 4 shows qualitative results on the DSIA test set, where our DMAligner most closely matches the ground truth.

4.3.2. Results on Sintel and DAVIS.

We conduct qualitative comparisons on the synthetic Sintel [2] dataset and the real-world DAVIS [36] dataset to evaluate the cross-domain performance of DMAligner and DSIA dataset. All competing methods and our DMAligner are trained on DSIA, and alignment results are di-

rectly tested on the Sintel Clean, Sintel Final training sets, and the DAVIS dataset. As there is no ground truth for precise evaluation, we calculate the feature distances between I_{pred} and I_1 using LPIPS and DreamSim [9]. Tab. 3 presents the quantitative results on Sintel and DAVIS, where DMAligner achieves the best average LPIPS and DreamSim scores. Fig. 6 shows examples from the DAVIS, and Fig. 5 displays results from the Sintel. These results demonstrate that DMAligner delivers exceptional image alignment performance in both synthetic and real-world scenarios.

4.3.3. Results on Downstream HDR Task.

In HDR imaging [49], LDR frames with alternating exposures (e.g., L_{t-1}, L_t, L_{t+1}) are aligned using flow warping before fusion. We replace this step with DMAligner, which aligns foreground and background more robustly, generating warped frames ($L_{t+1 \rightarrow t}, L_{t-1 \rightarrow t}$). Importantly, the fusion network and overall pipeline remain unchanged—only the aligned inputs differ. In Fig. 7, our method produces fewer artifacts, demonstrating strong generalization with existing HDR fusion networks.

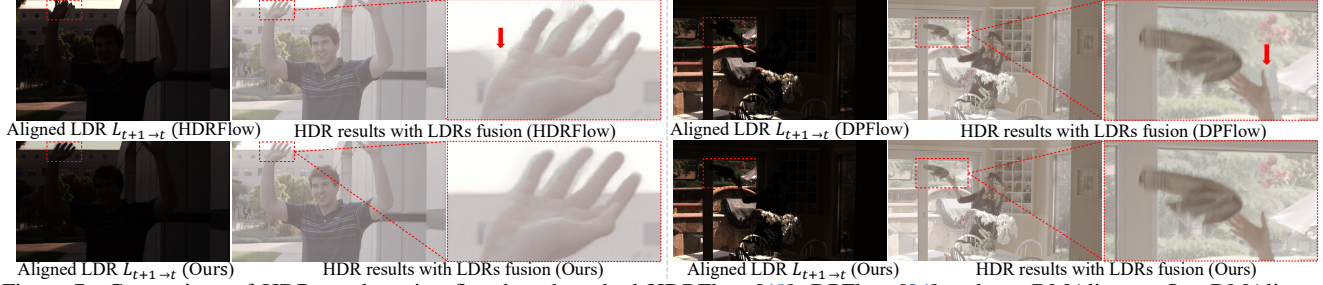


Figure 7. Comparison of HDR results using flow-based method HDRFlow [49], DPFlow [34] and our DMAligner. Our DMAligner significantly reduces ghosting and background distortions, especially around occluded regions and moving objects.

Table 3. Quantitative comparison on Sintel and DAVIS dataset. Due to the lack of ground truth for precise evaluation, we compute LPIPS and DreamSim [9] between I_{pred} and I_1 . Lower scores indicate better performance.

Methods	Sintel (Clean)		Sintel (Final)		DAVIS		Avg.	
	LPIPS↓	DreamSim↓	LPIPS↓	DreamSim↓	LPIPS↓	DreamSim↓	LPIPS↓	DreamSim↓
<i>Methods based on Flow Warping</i>								
PWCNet [44]	0.251	0.146	<u>0.177</u>	0.109	0.217	0.102	0.215	0.119
RAFT [45]	0.245	0.141	0.171	<u>0.102</u>	0.219	0.104	<u>0.212</u>	0.116
FlowFormer++ [42]	0.264	0.150	0.184	0.113	0.224	0.106	0.224	0.123
FlowDiffuser [28]	0.258	0.141	0.179	0.103	0.211	0.090	0.216	0.111
DPFlow [34]	0.255	<u>0.138</u>	0.178	0.101	<u>0.209</u>	<u>0.087</u>	0.214	<u>0.109</u>
<i>Methods based on View Synthesis</i>								
COGS [14]	0.411	0.172	0.378	0.131	0.398	0.121	0.396	0.142
SD-Inpaint [53]	0.269	0.164	0.271	0.142	0.241	0.114	0.260	0.140
GenWarp [41]	0.264	0.152	0.251	0.130	0.234	0.108	0.250	0.130
DMAligner (Ours)	<u>0.246</u>	0.123	0.186	0.117	0.202	0.084	0.211	0.108

Table 4. Ablation studies of predict targets and our DMP.

Exp.	Predict Targets	DMP	Avg	
			PSNR	SSIM
(a)	pred \hat{e}_t	w/o	24.82	0.77
(b)	pred x_0	w/o	25.12	0.79
(c)	rectified flow	w/	25.98	0.80
(d)	v-prediction	w/	26.16	0.81
(e)	pred x_0	w/	26.67	0.81

Ablation Study. Tab. 4 ablates prediction targets and DMP. Experiments (a)-(e) show that “predict x_0 ” achieves better alignment by directly targeting image reconstruction. Besides, (b) vs. (e) demonstrates that DMP enhances alignment by focusing the model on relevant dynamic regions.

Robustness Analysis. Stress tests in Fig. 8 reveal that DMAligner maintains a slower degradation rate and outperforms others even under large motion magnitude gaps.

5. Conclusion

This work represents a significant paradigm shift in image alignment by introducing a generation-based solution. The proposed DMAligner framework, a diffusion-based approach for image alignment through alignment-oriented view synthesis, effectively addresses challenges such as ghosting artifacts, occlusions, and illumination changes that previous methods struggle with. Notably, a Dynamics-aware Mask Producing (DMP) module is introduced to en-

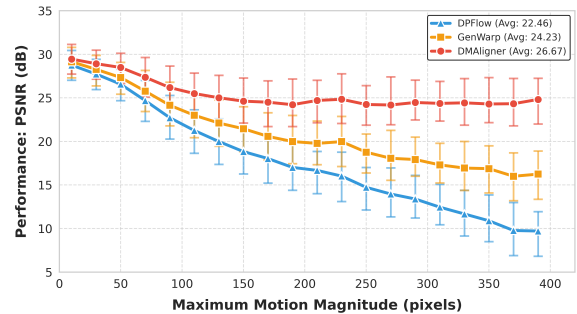


Figure 8. Stress test: performance vs. motion magnitude.

able the diffusion model to better handle dynamic foreground regions that are prone to errors. Additionally, the Dynamic Scene Image Alignment (DSIA) dataset is developed specifically for training. Extensive experiments demonstrate that DMAligner outperforms previous methods with strong cross-domain capabilities, excelling in both synthetic and real-world scenarios.

Acknowledgements. This work was supported by Sichuan Science and Technology Program under grant No. 2025ZYD0181, in part by the National Natural Science Foundation of China (NSFC) under grant Nos. 62372091 and 62402402, in part by the Hainan Province Science and Technology Plan Project under Grant ZDYF2024(LALH)001, and in part by the Fundamental Research Funds for the Central Universities under grant No. 2682025CX116.

References

- [1] Goutam Bhat, Martin Danelljan, Fisher Yu, Luc Van Gool, and Radu Timofte. Deep reparametrization of multi-frame super-resolution and denoising. *Proc. ICCV*, 2021. 2
- [2] Daniel J Butler, Jonas Wulff, Garrett B Stanley, and Michael J Black. A naturalistic open source movie for optical flow evaluation. *Proc. ECCV*, 2012. 2, 7
- [3] Kelvin CK Chan, Xintao Wang, Ke Yu, Chao Dong, and Chen Change Loy. Understanding deformable alignment in video super-resolution. *Proc. AAAI*, 2021. 1
- [4] Rufeng Chen, Bolun Zheng, Hua Zhang, Quan Chen, Cheng-gang Yan, Gregory Slabaugh, and Shanxin Yuan. Improving dynamic hdr imaging with fusion transformer. *Proc. AAAI*, 2023. 2
- [5] Cheng Chi, Siyuan Feng, Yilun Du, Zhenjia Xu, Eric Cousineau, Benjamin Burchfiel, and Shuran Song. Diffusion policy: Visuomotor policy learning via action diffusion. *Proceedings of Robotics: Science and Systems (RSS)*, 2023. 3
- [6] Changxing Deng, Ao Luo, Haibin Huang, Shaodan Ma, Jiangyu Liu, and Shuaicheng Liu. Explicit motion disentangling for efficient optical flow estimation. *Proc. ICCV*, 2023. 3
- [7] Zhenyan Ding, Zhixiang Fang, Zhengning Wang, Lehan Ding, Zhenni Zeng, Xinglong Luo, Shaoqin Yuan, Haoran Ma, and Binqun Leng. Lpudc: A laplacian pyramid neural network for restoring images from under-display cameras. *Neurocomputing*, 2025. 1
- [8] Akshay Dudhane, Syed Waqas Zamir, Salman Khan, Fahad Shahbaz Khan, and Ming-Hsuan Yang. Burst image restoration and enhancement. *Proc. CVPR*, 2022. 1
- [9] Stephanie Fu, Netanel Tamir, Shobhita Sundaram, Lucy Chai, Richard Zhang, Tali Dekel, and Phillip Isola. Dreamsim: Learning new dimensions of human visual similarity using synthetic data. *Proc. NeurIPS*, 2023. 7, 8
- [10] Klaus Greff, Francois Belletti, Lucas Beyer, Carl Doersch, Yilun Du, Daniel Duckworth, David J Fleet, Dan Gnanaprasam, Florian Golemo, Charles Herrmann, et al. Kubric: A scalable dataset generator. *Proc. CVPR*, 2022. 3
- [11] Jonathan Ho, Ajay Jain, and Pieter Abbeel. Denoising diffusion probabilistic models. *Proc. NeurIPS*, 2020. 3, 4
- [12] Hai Jiang, Ao Luo, Haoqiang Fan, Songchen Han, and Shuaicheng Liu. Low-light image enhancement with wavelet-based diffusion models. *ACM Trans. Graphics*, 2023. 3
- [13] Hai Jiang, Ao Luo, Xiaohong Liu, Songchen Han, and Shuaicheng Liu. Lightendiffusion: Unsupervised low-light image enhancement with latent-retinex diffusion models. *Proc. ECCV*, 2024. 3
- [14] Kaiwen Jiang, Yang Fu, Mukund Varma T, Yash Belhe, Xiaolong Wang, Hao Su, and Ravi Ramamoorthi. A construct-optimize approach to sparse view synthesis without camera pose. *Proc. ACM SIGGRAPH*, 2024. 5, 6, 8
- [15] Bingxin Ke, Anton Obukhov, Shengyu Huang, Nando Metzger, Rodrigo Caye Daudt, and Konrad Schindler. Repurposing diffusion-based image generators for monocular depth estimation. *Proc. CVPR*, 2024. 6
- [16] Haipeng Li, Hai Jiang, Ao Luo, Ping Tan, Haoqiang Fan, Bing Zeng, and Shuaicheng Liu. Dmhom: Learning homography with diffusion models. *ACM Trans. Graphics*, 2024. 3
- [17] Zhengqi Li, Tali Dekel, Forrester Cole, Richard Tucker, Noah Snavely, Ce Liu, and William T Freeman. Learning the depths of moving people by watching frozen people. *Proc. CVPR*, 2019. 3
- [18] Ce Liu, Jenny Yuen, and Antonio Torralba. Sift flow: Dense correspondence across scenes and its applications. *IEEE Trans. on Pattern Analysis and Machine Intelligence*, 2010. 2
- [19] Shuaicheng Liu, Ping Tan, Lu Yuan, Jian Sun, and Bing Zeng. Meshflow: Minimum latency online video stabilization. *Proc. ECCV*, 2016. 6
- [20] Shuaicheng Liu, Yuhang Lu, Hai Jiang, Nianjin Ye, Chuan Wang, and Bing Zeng. Unsupervised global and local homography estimation with motion basis learning. *IEEE Trans. on Pattern Analysis and Machine Intelligence*, 2022. 2, 3
- [21] Shuaicheng Liu, Nianjin Ye, Chuan Wang, Jirong Zhang, Lanpeng Jia, Kunming Luo, Jue Wang, and Jian Sun. Content-aware unsupervised deep homography estimation and its extensions. *IEEE Trans. on Pattern Analysis and Machine Intelligence*, 2022. 2, 3
- [22] Shuaicheng Liu, Zhuofan Zhang, Zhen Liu, Ping Tan, and Bing Zeng. Minimum latency deep online video stabilization and its extensions. *IEEE Trans. on Pattern Analysis and Machine Intelligence*, 2025. 1
- [23] Zhen Liu, Wenjie Lin, Xinpeng Li, Qing Rao, Ting Jiang, Mingyan Han, Haoqiang Fan, Jian Sun, and Shuaicheng Liu. Adnet: Attention-guided deformable convolutional network for high dynamic range imaging. *Proc. CVPRW*, 2021. 2
- [24] Zhen Liu, Yinglong Wang, Bing Zeng, and Shuaicheng Liu. Ghost-free high dynamic range imaging with context-aware transformer. *Proc. ECCV*, 2022. 3
- [25] Zhen Liu, Hai Jiang, Haipeng Li, Shuaicheng Liu, and Bing Zeng. Solving ill-posed regions in high dynamic range reconstruction with uncertainty-aware diffusion models. *IEEE Trans. on Circuits and Systems for Video Technology*, 2025. 3
- [26] Zhen Liu, Diedong Feng, Hai Jiang, Liaoyuan Zeng, Hao Wang, Chaoyu Feng, Lei Lei, Bing Zeng, and Shuaicheng Liu. Raw-flow: Advancing rgb-to-raw image reconstruction with deterministic latent flow matching. *Proc. AAAI*, 2026. 3
- [27] Ao Luo, Fan Yang, Xin Li, Lang Nie, Chunyu Lin, Haoqiang Fan, and Shuaicheng Liu. Gaflow: Incorporating gaussian attention into optical flow. *Proc. ICCV*, 2023. 3
- [28] Ao Luo, Xin Li, Fan Yang, Jiangyu Liu, Haoqiang Fan, and Shuaicheng Liu. Flowdiffuser: Advancing optical flow estimation with diffusion models. *Proc. CVPR*, 2024. 3, 5, 6, 8
- [29] Jinting Luo, Ru Li, Chengzhi Jiang, Xiaoming Zhang, Mingyan Han, Ting Jiang, Haoqiang Fan, and Shuaicheng Liu. Diff-shadow: Global-guided diffusion model for shadow removal. *Proc. AAAI*, 2025. 3

- [30] Xinglong Luo, Kunming Luo, Ao Luo, Zhengning Wang, Ping Tan, and Shuaicheng Liu. Learning optical flow from event camera with rendered dataset. *Proc. ICCV*, 2023. 3
- [31] Xinglong Luo, Ao Luo, Zhengning Wang, Chunyu Lin, Bing Zeng, and Shuaicheng Liu. Efficient meshflow and optical flow estimation from event cameras. *Proc. CVPR*, 2024. 6
- [32] Xinglong Luo, Ao Luo, Kunming Luo, Zhengning Wang, Ping Tan, Bing Zeng, and Shuaicheng Liu. Learning efficient meshflow and optical flow from event cameras. *IEEE Trans. on Pattern Analysis and Machine Intelligence*, 2025. 6
- [33] Mao Mao, Xujie Shen, Guyuan Chen, Boming Zhao, Jiarui Hu, Hujun Bao, and Zhaopeng Cui. Accidentalgs: 3d gaussian splatting from accidental camera motion. In *Proc. ICCV*, 2025. 5, 6
- [34] Henrique Morimitsu, Xiaobin Zhu, Roberto M. Cesar, Xiangyang Ji, and Xu-Cheng Yin. Dpflow: Adaptive optical flow estimation with a dual-pyramid framework. *Proc. CVPR*, 2025. 5, 6, 7, 8
- [35] Sicheng Pan and Yingming Li. Ebdnet: Integrating optical flow with kernel prediction for burst denoising. *IEEE Trans. on Circuits and Systems for Video Technology*, 2024. 1
- [36] F. Perazzi, J. Pont-Tuset, B. McWilliams, L. Van Gool, M. Gross, and A. Sorkine-Hornung. A benchmark dataset and evaluation methodology for video object segmentation. *Proc. CVPR*, 2016. 2, 7
- [37] Yang Ren, Hai Jiang, Wei Li, Menglong Yang, Heng Zhang, Zehua Sheng, Qingsheng Ye, and Shuaicheng Liu. Learning arbitrary-scale raw image downscaling with wavelet-based recurrent reconstruction. *Proc. ACM Multimedia*, 2025. 3
- [38] Yang Ren, Hai Jiang, Menglong Yang, Wei Li, and Shuaicheng Liu. Ispdiffuser: Learning raw-to-srgb mappings with texture-aware diffusion models and histogram-guided color consistency. *Proc. AAAI*, 2025. 3
- [39] Yang Ren, Xinhan Niu, Hai Jiang, Zhen Liu, Ting Jiang, Guanghui Liu, and Shuaicheng Liu. Ispformer: Learning raw-to-srgb mappings with wavelet-based self-attention. *Neurocomputing*, 2025. 3
- [40] Robin Rombach, Andreas Blattmann, Dominik Lorenz, Patrick Esser, and Björn Ommer. High-resolution image synthesis with latent diffusion models. *Proc. CVPR*, 2022. 2, 3, 6
- [41] Junyoung Seo, Kazumi Fukuda, Takashi Shibuya, Takuya Narihira, Naoki Murata, Shoukang Hu, Chieh-Hsin Lai, Seungryoung Kim, and Yuki Mitsufuji. Genwarp: Single image to novel views with semantic-preserving generative warping. *Proc. NeurIPS*, 2024. 5, 6, 7, 8
- [42] Xiaoyu Shi, Zhaoyang Huang, Dasong Li, Manyuan Zhang, Ka Chun Cheung, Simon See, Hongwei Qin, Jifeng Dai, and Hongsheng Li. Flowformer++: Masked cost volume autoencoding for pretraining optical flow estimation. *Proc. CVPR*, 2023. 5, 6, 8
- [43] Jiaming Song, Chenlin Meng, and Stefano Ermon. Denoising diffusion implicit models. *Proc. ICLR*, 2021. 3, 5
- [44] Deqing Sun, Xiaodong Yang, Ming-Yu Liu, and Jan Kautz. Pwc-net: Cnns for optical flow using pyramid, warping, and cost volume. *Proc. ICCV*, 2018. 5, 6, 8
- [45] Zachary Teed and Jia Deng. Raft: Recurrent all-pairs field transforms for optical flow. *Proc. ECCV*, 2020. 5, 6, 8
- [46] Zhengning Wang, Xuhang Liu, Chuan Wang, Ting Jiang, Tianjiao Zeng, Zhenni Zeng, Guoqing Wang, and Shuaicheng Liu. Reconstruction flow recurrent network for compressed video quality enhancement. *Pattern Recognition*, 2024. 1
- [47] Chongyang Xu, Shen Cheng, Haipeng Li, Haoqiang Fan, Ziliang Feng, and Shuaicheng Liu. Hero: Hierarchical 3d semantic representation for pose-aware object manipulation. *arXiv preprint arXiv:2602.18817*, 2026. 3
- [48] Chongyang Xu, Haipeng Li, Shen Cheng, Jingyu Hu, Haoqiang Fan, Ziliang Feng, and Shuaicheng Liu. Action-geometry prediction with 3d geometric prior for bimanual manipulation. *arXiv preprint arXiv:2602.23814*, 2026. 3
- [49] Gangwei Xu, Yujin Wang, Jinwei Gu, Tianfan Xue, and Xin Yang. Hdrflow: Real-time hdr video reconstruction with large motions. *Proc. CVPR*, 2024. 1, 7, 8
- [50] Haofei Xu, Jing Zhang, Jianfei Cai, Hamid Rezaatofighi, and Dacheng Tao. Gmflow: Learning optical flow via global matching. *Proc. CVPR*, 2022. 6, 7
- [51] Zhanglei Yang, Haipeng Li, Mingbo Hong, Chen-Lin Zhang, Jiajun Li, and Shuaicheng Liu. Single image rolling shutter removal with diffusion models. *Proc. AAAI*, 2025. 3
- [52] Geunhyuk Youk, Jihyong Oh, and Munchurl Kim. Fmanet: Flow-guided dynamic filtering and iterative feature refinement with multi-attention for joint video super-resolution and deblurring. *Proc. CVPR*, 2024. 1
- [53] Jason J Yu, Fereshteh Forghani, Konstantinos G Derpanis, and Marcus A Brubaker. Long-term photometric consistent novel view synthesis with diffusion models. *Proc. ICCV*, 2023. 6, 8
- [54] Qihang Yu, Ju He, Xueqing Deng, Xiaohui Shen, and Liang-Chieh Chen. Convolutions die hard: Open-vocabulary segmentation with single frozen convolutional clip. *Proc. NeurIPS*, 2023. 6
- [55] Huanjing Yue, Cong Cao, Lei Liao, Ronghe Chu, and Jingyu Yang. Supervised raw video denoising with a benchmark dataset on dynamic scenes. *Proc. CVPR*, 2020. 1
- [56] Jiawei Zhang, Jinshan Pan, Daoye Wang, Shangchen Zhou, Xing Wei, Furong Zhao, Jianbo Liu, and Jimmy Ren. Deep dynamic scene deblurring from optical flow. *IEEE Trans. on Circuits and Systems for Video Technology*, 2021. 3
- [57] Qinglun Zhang, Zhen Liu, Haoqiang Fan, Guanghui Liu, Bing Zeng, and Shuaicheng Liu. Flowpolicy: Enabling fast and robust 3d flow-based policy via consistency flow matching for robot manipulation. *Proc. AAAI*, 2025. 3
- [58] Jianwei Zhao, Xin Li, Fan Yang, Qiang Zhai, Ao Luo, Zicheng Jiao, and Hong Cheng. Focusdiffuser: Perceiving local disparities for camouflaged object detection. *Proc. ECCV*, 2024. 3
- [59] Yang Zheng, Adam W Harley, Bokui Shen, Gordon Wetstein, and Leonidas J Guibas. Pointodyssey: A large-scale synthetic dataset for long-term point tracking. *Proc. ICCV*, 2023. 3
- [60] Tianhao Zhou, Haipeng Li, Ziyi Wang, Ao Luo, Chen-Lin Zhang, Jiajun Li, Bing Zeng, and Shuaicheng Liu. Recdiffusion: Rectangling for image stitching with diffusion models. *Proc. CVPR*, 2024. 3